

Tripartite entanglement and threshold properties of coupled intracavity down-conversion and sum-frequency generation

C. Pennarun,^{1,2} A. S. Bradley,¹ and M. K. Olsen¹¹ARC Centre of Excellence for Quantum-Atom Optics, School of Physical Sciences, University of Queensland, Brisbane, QLD 4072, Australia²Ecole Normale Supérieure de Physique de Grenoble, Institut National Polytechnique, Grenoble, France

(Received 22 August 2007; published 14 December 2007)

The process of cascaded down-conversion and sum-frequency generation inside an optical cavity has been predicted to be a potential source of three-mode continuous-variable entanglement. When the cavity is pumped by two fields, the threshold properties have been analyzed, showing that these are more complicated than in well-known processes such as optical parametric oscillation. When there is only a single pumping field, the entanglement properties have been calculated using a linearized fluctuation analysis, but without any consideration of the threshold properties or critical operating points of the system. In this work we extend this analysis to demonstrate that the singly pumped system demonstrates a rich range of threshold behavior when quantization of the pump field is taken into account and that asymmetric polychromatic entanglement is available over a wide range of operational parameters.

DOI: [10.1103/PhysRevA.76.063812](https://doi.org/10.1103/PhysRevA.76.063812)

PACS number(s): 42.65.Lm, 42.50.Dv, 03.65.Ud, 03.67.Mn

I. INTRODUCTION

The modern field of quantum information originally focused on what is known as discrete-variable entanglement and developed to include the study of entanglement between continuous-variable phase quadratures of the electromagnetic field, which have a close analogy with the original position and momentum considered in the famous Einstein-Podolsky-Rosen (EPR) paradox [1]. In the beginning this research considered bipartite entanglement as produced by, for example, the optical parametric oscillator (OPO) [2] and led to experimental demonstrations of the EPR paradox [3] and of what is known as continuous-variable quantum teleportation [4–6]. Many systems have now been studied, both theoretically and experimentally, with continuous-variable bipartite entanglement now considered an important resource for quantum information applications [7].

Recently there has been much attention paid to the production of continuous-variable tripartite entanglement, obtained either by mixing squeezed beams on unbalanced beamsplitters [8,9], or via the interaction of multiple input beams in nonlinear media with cascaded or concurrent $\chi^{(2)}$ nonlinearities. Among the latter are systems using either single [10], twin [11–15], or triple [16–18] nonlinearities. These nonlinear processes have been analyzed and demonstrated in both the traveling-wave and intracavity configurations. In this work we are interested in an intracavity process which combines parametric down-conversion with sum frequency generation, as theoretically analyzed by Yu *et al.* [19]. The idea of combining these two processes is due to Smithers and Lu [20], who did not consider enclosing the processes in an optical cavity. The intracavity process with two pump fields was first analyzed by Guo *et al.* [12], who used quantum Langevin equations [21] with an undepleted pump approximation, which can give no insight into threshold behavior or any critical operating points. An analysis which included quantization of the two pump fields was performed by Olsen and Bradley [13], demonstrating that the

system had quite different stability and threshold behaviors to the normal OPO. As Yu *et al.* [19] have also used an undepleted pump approximation (also known as the parametric approximation) and quantum Langevin equations for the singly pumped intracavity system, they are not able to determine the threshold behaviors or the stability of the equations they use. In this paper we apply a fully quantized treatment of all the interacting fields, finding that there are two separate parameter regimes, one of which has an oscillation threshold while the other does not. The reason for this behavior, which is more complicated than that of the standard OPO, is that down-conversion considered separately does exhibit a threshold while sum frequency conversion does not. As we will demonstrate below, it is the competition and interplay of these two processes that leads to more complicated behavior.

II. HAMILTONIAN AND EQUATIONS OF MOTION

Our system is a nonlinear medium inside an optical cavity that is pumped at frequency ω_0 and is resonant at all the frequencies involved. In Yu *et al.* [19] the nonlinear medium is a quasiperiodic superlattice. In the down-conversion part of the intracavity process, two fields at ω_1 and ω_3 are generated, where $\omega_0 = \omega_1 + \omega_3$. We will denote the effective nonlinearity for this process by χ_1 . The pump field at ω_0 can then combine with the field at ω_3 in a sum frequency generation process, to produce a further field at ω_2 , with the effective nonlinearity represented as χ_2 . We will use the annihilation operator \hat{b} to describe the field at ω_0 , while the operators \hat{a}_j will be used for the fields at ω_j .

The Hamiltonian can be written as

$$\hat{H}_{\text{tot}} = \hat{H}_{\text{pump}} + \hat{H}_{\text{int}} + \hat{H}_{\text{damp}}, \quad (1)$$

where the interaction Hamiltonian is

$$\hat{H}_{\text{int}} = i\hbar\chi_1(\hat{b}\hat{a}_1^\dagger\hat{a}_3^\dagger - \hat{b}^\dagger\hat{a}_1\hat{a}_3) + i\hbar\chi_2(\hat{b}\hat{a}_3\hat{a}_2^\dagger - \hat{b}^\dagger\hat{a}_3^\dagger\hat{a}_2), \quad (2)$$

the Hamiltonian describing the cavity pumping is

$$\hat{H}_{\text{pump}} = i\hbar(\epsilon\hat{b}^\dagger - \epsilon^*\hat{b}), \quad (3)$$

and the cavity damping Hamiltonian is

$$\hat{H}_{\text{damp}} = \hbar(\hat{\Gamma}_0\hat{b}^\dagger + \hat{\Gamma}_0^\dagger\hat{b}) + \hbar\sum_{j=1:3}(\hat{\Gamma}_j\hat{a}_j^\dagger + \hat{\Gamma}_j^\dagger\hat{a}_j). \quad (4)$$

In the above, ϵ is the pump field that enters the cavity, which will be described classically, and the $\hat{\Gamma}_j$ are reservoir operators for each of the intracavity modes.

We can gain some intuition about the behavior of the system by inspection of the interaction Hamiltonian of 2 in isolation from the rest of the total Hamiltonian. The part containing χ_1 describes the well-known process of nondegenerate down-conversion and produces twin photons at the frequencies ω_1 and ω_3 . If χ_2 were absent, this would produce bipartite entangled modes at these frequencies, the behavior of which has been exhaustively studied. As there is also a term proportional to χ_2 that combines a photon in one of these modes (ω_3) with a pump photon to produce a photon at

ω_2 , we may expect that the bipartite entanglement produced by the χ_1 interaction will be a little degraded. However, it is through this process that tripartite entanglement is made available by the relationship between the modes at ω_2 and ω_3 . As with the harmonic entanglement produced in traveling wave second harmonic generation [22], we do not expect that sum frequency generation will violate the entanglement measures by as much as coupled down-conversion processes can. It is this basic asymmetry between the two processes that makes a careful choice of entanglement criteria necessary and changes the threshold properties once the cavity dynamics are included, as we will now proceed to investigate more quantitatively.

To calculate the fluctuation and entanglement properties of the system we will derive fully quantum equations of motion using the positive- P pseudoprobability distribution [23], as this naturally allows us to calculate the normally ordered operator expectation values required to find output spectra. Proceeding via the normal methods [24] and making the zero temperature and Markov approximations for the reservoir [25], we find the Fokker-Planck equation for the P function [26,27] of the system as

$$\begin{aligned} \frac{dP}{dt} = & \left\{ - \left[\frac{\partial}{\partial\alpha_1}(\gamma_1\alpha_1 - \chi_1\alpha_3^*\beta) + \frac{\partial}{\partial\alpha_1^*}(\gamma_1\alpha_1^* - \chi_1\alpha_3\beta^*) + \frac{\partial}{\partial\alpha_2}(\gamma_2\alpha_2 - \chi_2\alpha_3\beta) + \frac{\partial}{\partial\alpha_2^*}(\gamma_2\alpha_2^* - \chi_2\alpha_3^*\beta^*) \right. \right. \\ & + \frac{\partial}{\partial\alpha_3}(\gamma_3\alpha_3 - \chi_1\alpha_1^*\beta + \chi_2\alpha_2\beta^*) + \frac{\partial}{\partial\alpha_3^*}(\gamma_3\alpha_3^* - \chi_1\alpha_1\beta^* + \chi_2\alpha_2^*\beta) + \frac{\partial}{\partial\beta}(\gamma_0\beta - \epsilon + \chi_1\alpha_1\alpha_3 + \chi_2\alpha_2\alpha_3^*) \\ & \left. \left. + \frac{\partial}{\partial\beta^*}(\gamma_0\beta^* - \epsilon^* + \chi_1\alpha_1^*\alpha_3^* + \chi_2\alpha_2^*\alpha_3) \right] + \frac{1}{2} \left[2\chi_1 \left(\frac{\partial^2}{\partial\alpha_1\partial\alpha_3}\beta + \frac{\partial^2}{\partial\alpha_1^*\partial\alpha_3^*}\beta^* \right) - 2\chi_2 \left(\frac{\partial^2}{\partial\alpha_3\partial\beta}\alpha_2^* + \frac{\partial^2}{\partial\alpha_3^*\partial\beta^*}\alpha_2 \right) \right] \right\} P, \quad (5) \end{aligned}$$

where the γ_j are the cavity loss rates at frequency ω_j . As this Fokker-Planck equation does not possess a positive-definite diffusion matrix, we must double the phase space and use the positive- P representation to find the appropriate stochastic differential equations. This results in replacement of the conjugate variables by α_j^+ and β^+ , which are the complex conjugates of the uncrossed variables only in the mean. Stochastic averages of products of these variables are then equal to normally ordered expectation values of the corresponding operators. We find the coupled set of stochastic differential equations as

$$\frac{d\alpha_1}{dt} = -\gamma_1\alpha_1 + \chi_1\alpha_3^+\beta + \sqrt{\frac{\chi_1\beta}{2}}(\eta_1 + i\eta_2),$$

$$\frac{d\alpha_1^+}{dt} = -\gamma_1\alpha_1^+ + \chi_1\alpha_3\beta^+ + \sqrt{\frac{\chi_1\beta^+}{2}}(\eta_3 + i\eta_4),$$

$$\frac{d\alpha_2}{dt} = -\gamma_2\alpha_2 + \chi_2\alpha_3\beta,$$

$$\frac{d\alpha_2^+}{dt} = -\gamma_2\alpha_2^+ + \chi_2\alpha_3^+\beta^+,$$

$$\begin{aligned} \frac{d\alpha_3}{dt} = & -\gamma_3\alpha_3 + \chi_1\alpha_1^+\beta - \chi_2\alpha_2\beta^+ + \sqrt{\frac{\chi_1\beta}{2}}(\eta_1 - i\eta_2) \\ & + \sqrt{-\frac{\chi_2\alpha_2^+}{2}}(\eta_5 + i\eta_6), \end{aligned}$$

$$\begin{aligned} \frac{d\alpha_3^+}{dt} = & -\gamma_3\alpha_3^+ + \chi_1\alpha_1\beta^+ - \chi_2\alpha_2^+\beta + \sqrt{\frac{\chi_1\beta^+}{2}}(\eta_3 - i\eta_4) \\ & + \sqrt{-\frac{\chi_2\alpha_2}{2}}(\eta_7 + i\eta_8), \end{aligned}$$

$$\frac{d\beta}{dt} = \epsilon - \gamma_0\beta - \chi_1\alpha_1\alpha_3 - \chi_2\alpha_2\alpha_3^+ + \sqrt{-\frac{\chi_2\alpha_2^+}{2}}(\eta_5 - i\eta_6),$$

$$\frac{d\beta^+}{dt} = \epsilon^* - \gamma_0\beta^+ - \chi_1\alpha_1^+\alpha_3^+ - \chi_2\alpha_2^+\alpha_3 + \sqrt{\frac{-\chi_2\alpha_2}{2}}(\eta_7 - i\eta_8), \quad (6)$$

where the η_j are real Gaussian noise terms with the properties

$$\overline{\eta_j(t)} = 0, \overline{\eta_j(t)\eta_k(t')} = \delta_{jk}\delta(t-t'). \quad (7)$$

In cases where the procedure is valid, the noise terms may be dropped and the resulting semiclassical equations linearized about their steady states, which results in the process being treated as an Ornstein-Uhlenbeck process [28], allowing for easy calculation of the output spectra. The validity of this linearized fluctuation analysis is usually found by calculating the eigenvalues of the resulting drift matrix for the fluctuations and requires knowledge of the classical steady-state solutions. In fact, in the present case, we find that stochastic integration of the above equations presents various stability problems in the regions where they cannot be linearized, so that in Sec. VI we will turn to the truncated Wigner representation [29] to find time domain solutions in these parameter regimes.

III. LINEARIZED FLUCTUATION ANALYSIS

In the steady state, we can always decompose the system variables into their mean values and a part which fluctuates about these. In many cases the mean value solutions of the noiseless equations are equal to the operator expectation values and the fluctuations can be treated as being stable and Gaussian about zero means. In these cases we may use this linearized fluctuation analysis as a simple method to calculate measurable spectra. We will perform this process on the positive- P equations, beginning with the decomposition $\alpha_i = \bar{\alpha}_i + \delta\alpha_i$ and similarly for β . This gives us the set of equations for the fluctuating terms

$$\frac{d}{dt}\delta\alpha_1 = -\gamma_1\delta\alpha_1 + \chi_1\bar{\beta}\delta\alpha_3^* + \sqrt{\frac{\chi_1\bar{\beta}}{2}}(\eta_1 + i\eta_2),$$

$$\frac{d}{dt}\delta\alpha_1^* = -\gamma_1\delta\alpha_1^* + \chi_1\bar{\beta}^*\delta\alpha_3 + \sqrt{\frac{\chi_1\bar{\beta}^*}{2}}(\eta_3 + i\eta_4),$$

$$\frac{d}{dt}\delta\alpha_2 = -\gamma_2\delta\alpha_2 + \chi_2\bar{\beta}\delta\alpha_3,$$

$$\frac{d}{dt}\delta\alpha_2^* = -\gamma_2\delta\alpha_2^* + \chi_2\bar{\beta}^*\delta\alpha_3^*,$$

$$\frac{d}{dt}\delta\alpha_3 = -\gamma_3\delta\alpha_3 + \chi_1\bar{\beta}\delta\alpha_1^* - \chi_2\bar{\beta}^*\delta\alpha_2 + \sqrt{\frac{\chi_1\bar{\beta}}{2}}(\eta_1 - i\eta_2),$$

$$\frac{d}{dt}\delta\alpha_3^* = -\gamma_3\delta\alpha_3^* + \chi_1\bar{\beta}^*\delta\alpha_1 - \chi_2\bar{\beta}\delta\alpha_2^* + \sqrt{\frac{\chi_1\bar{\beta}^*}{2}}(\eta_3 - i\eta_4),$$

$$\frac{d}{dt}\delta\beta = -\gamma_0\delta\beta,$$

$$\frac{d}{dt}\delta\beta^* = -\gamma_0\delta\beta^*, \quad (8)$$

which may be written in matrix form for the vector

$$\delta\tilde{\alpha} = [\delta\alpha_1, \delta\alpha_1^*, \delta\alpha_2, \delta\alpha_2^*, \delta\alpha_3, \delta\alpha_3^*, \delta\beta, \delta\beta^*]^T \quad (9)$$

as

$$\frac{d}{dt}\delta\tilde{\alpha} = -A\delta\tilde{\alpha} + Bd\tilde{W}, \quad (10)$$

where A is the drift matrix, B contains the steady-state coefficients of the noise terms, and $d\tilde{W}$ is a vector of Wiener increments. The condition for stability of the fluctuations is that the eigenvalues of A have no negative real parts. When this condition is fulfilled, we may calculate the intracavity spectral matrix as

$$S(\omega) = (A + i\omega\mathbb{1})^{-1}BB^T(A^T - i\omega\mathbb{1})^{-1}, \quad (11)$$

which, along with the well-known input-output relations [21], allow us to calculate the measurable spectral quantities outside the cavity.

A. Steady-state classical solutions

The classical equations for the mean values are found as

$$\frac{d\bar{\alpha}_1}{dt} = -\gamma_1\bar{\alpha}_1 + \chi_1\bar{\alpha}_3^*\bar{\beta},$$

$$\frac{d\bar{\alpha}_2}{dt} = -\gamma_2\bar{\alpha}_2 + \chi_2\bar{\alpha}_3\bar{\beta},$$

$$\frac{d\bar{\alpha}_3}{dt} = -\gamma_3\bar{\alpha}_3 + \chi_1\bar{\alpha}_1^*\bar{\beta} - \chi_2\bar{\alpha}_2\bar{\beta}^*,$$

$$\frac{d\bar{\beta}}{dt} = \epsilon - \gamma_0\bar{\beta} - \chi_1\bar{\alpha}_1\bar{\alpha}_3 - \chi_2\bar{\alpha}_2\bar{\alpha}_3^*, \quad (12)$$

and may be solved for the steady-state solutions that enable us to perform the necessary stability analysis. We find that the solutions are divided into two different classes, depending on whether an oscillation threshold is present or not.

1. Regime with threshold

If $\chi_1^2\gamma_2 > \chi_2^2\gamma_1$, we find that the system has a threshold pumping value below which it will not oscillate. If the value of the pump field ϵ is below

$$\epsilon_c = \frac{\gamma_0\sqrt{\gamma_3}}{\sqrt{\frac{\chi_1^2}{\gamma_1} - \frac{\chi_2^2}{\gamma_2}}}, \quad (13)$$

the signal modes will not be macroscopically occupied. We note that this is totally different from the expression that would be expected if we considered the threshold for the down-conversion process in isolation, which would be given as $\epsilon_c^o = \gamma_0\sqrt{\gamma_1\gamma_3}/\chi_1$. This difference in threshold cannot be calculated in the approach taken by Yu *et al.* [19] and can be explained by the fact that the relative strengths of the couplings and cavity losses mean that as photons at ω_3 are absorbed to create photons at ω_2 , the latter exit the cavity on a short time scale. As sum frequency generation does not have a threshold, this means that ω_3 photons are either absorbed or lost before they can begin to oscillate macroscopically in the cavity, which also means that the mode at ω_1 cannot become macroscopically occupied below this modified threshold pumping rate. The analytical expressions for the different mean-value steady-state solutions are (note we will now drop the bar over the variables for notational convenience).

(i) $\epsilon < \epsilon_c$

$$\begin{aligned} \beta^{SS} &= \frac{\epsilon}{\gamma_0}, \\ \alpha_j^{SS} &= 0, \end{aligned} \quad (14)$$

where $j=1, 2, 3$.

(ii) $\epsilon > \epsilon_c$

$$\begin{aligned} \beta^{SS} &= \sqrt{\frac{\gamma_3}{\frac{\chi_1^2}{\gamma_1} - \frac{\chi_2^2}{\gamma_2}}}, \\ \alpha_1^{SS} &= \pm \frac{\chi_1}{\gamma_1} \beta^{SS} \sqrt{\frac{\epsilon - \epsilon_c}{\frac{\epsilon_c}{\gamma_0} \left(\frac{\chi_1^2}{\gamma_1} + \frac{\chi_2^2}{\gamma_2} \right)}} e^{-i\theta}, \\ \alpha_2^{SS} &= \pm \frac{\chi_2}{\gamma_2} \beta^{SS} \sqrt{\frac{\epsilon - \epsilon_c}{\frac{\epsilon_c}{\gamma_0} \left(\frac{\chi_1^2}{\gamma_1} + \frac{\chi_2^2}{\gamma_2} \right)}} e^{i\theta}, \\ \alpha_3^{SS} &= \pm \sqrt{\frac{\epsilon - \epsilon_c}{\frac{\epsilon_c}{\gamma_0} \left(\frac{\chi_1^2}{\gamma_1} + \frac{\chi_2^2}{\gamma_2} \right)}} e^{i\theta}, \end{aligned} \quad (15)$$

where θ is an undetermined phase. We notice that owing to the presence of the square root, the sign of these solutions is unknown. However, inspection shows that the square roots all have to be the same sign, whether this is positive or negative. Nevertheless, because the only phase we know is

the phase of the pump field ϵ , which we take as real, β^{SS} will also be real. As θ is not fixed, these above threshold solutions will exhibit phase diffusion, as previously found in the non-degenerate parametric oscillator [30].

2. Regime without threshold

We find that if $\chi_1^2\gamma_2 < \chi_2^2\gamma_1$ there is no threshold predicted by the classical equations, which means that for any value of the pump field the signal modes will not be macroscopically occupied. Some insight into this behavior can be given by considering the same arguments as given above for the threshold value in the region with an oscillation threshold and considering that the pumping rate must now be infinite to allow oscillation. The expressions for the steady-state solutions are the same as the below threshold solutions of the previous case,

$$\begin{aligned} \beta^{SS} &= \frac{\epsilon}{\gamma_0}, \\ \alpha_j^{SS} &= 0. \end{aligned} \quad (16)$$

In our analyses in this regime we will scale the pump amplitude by the normal OPO threshold $\epsilon_c^o = \gamma_0\sqrt{\gamma_1\gamma_3}/\chi_1$, so that the pump field ϵ will be expressed as a proportion of this threshold. Now that the classical steady-state values in the different areas are known, we can analyze the stability of the fluctuations.

B. Stability analysis

To determine the validity of the linearization process we will now analyze the eigenvalues of the drift matrix A of Eq. (10). This is written out in full as

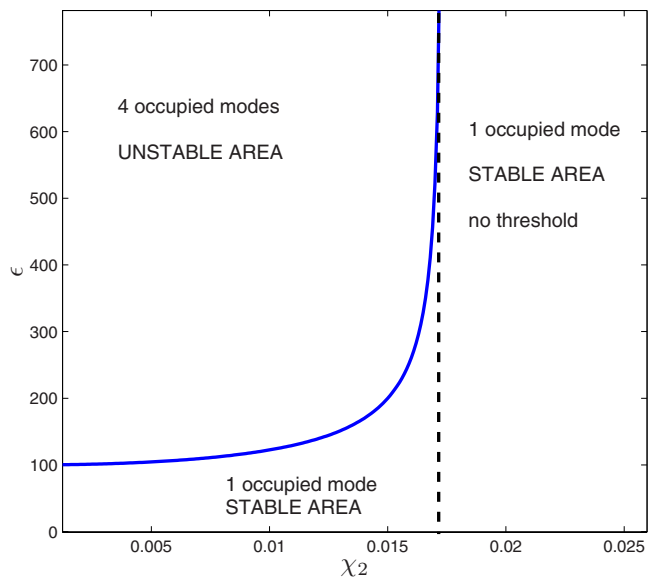


FIG. 1. (Color online) Stability of the steady state solutions with $\chi_1=0.01$, $\gamma_0=\gamma_1=\gamma_3=1$, and $\gamma_2=3$, as χ_2 and the pump amplitude are varied. The dashed line shows the separation between the system with and without threshold.

$$A = \begin{bmatrix} \gamma_1 & 0 & 0 & 0 & 0 & -\chi_1\beta^{SS} & -\chi_1\alpha_3^* & 0 \\ 0 & \gamma_1 & 0 & 0 & -\chi_1(\beta^{SS})^* & 0 & 0 & -\chi_1\alpha_3 \\ 0 & 0 & \gamma_2 & 0 & -\chi_2\beta^{SS} & 0 & -\chi_2\alpha_3^{SS} & 0 \\ 0 & 0 & 0 & \gamma_2 & 0 & -\chi_2(\beta^{SS})^* & 0 & -\chi_2(\alpha_3^{SS})^* \\ 0 & -\chi_1\beta^{SS} & \chi_2(\beta^{SS})^* & 0 & \gamma_3 & 0 & -\chi_1(\alpha_1^{SS})^* & \chi_2\alpha_2^{SS} \\ -\chi_1(\beta^{SS})^* & 0 & 0 & \chi_2\beta^{SS} & 0 & \gamma_3 & \chi_2(\alpha_2^{SS})^* & -\chi_1\alpha_1^{SS} \\ \chi_1\alpha_3^{SS} & 0 & \chi_2(\alpha_3^{SS})^* & 0 & \chi_1\alpha_1^{SS} & \chi_2\alpha_2^{SS} & \gamma_0 & 0 \\ 0 & \chi_1(\alpha_3^{SS})^* & 0 & \chi_2\alpha_3^{SS} & \chi_2(\alpha_2^{SS})^* & \chi_1(\alpha_1^{SS})^* & 0 & \gamma_0 \end{bmatrix}. \quad (17)$$

The analytical expressions for the eigenvalues of the matrix A above threshold are not easily obtained, but below threshold where all the α_j^{SS} are zero and $\beta^{SS} = \epsilon / \gamma_0$, we find the characteristic polynomial as

$$(\gamma_0 - \lambda)^2 [(\gamma_1 - \lambda)(\gamma_2 - \lambda)(\gamma_3 - \lambda) + \lambda(\beta^{SS})^2(\chi_1^2 - \chi_2^2) + (\beta^{SS})^2(\gamma_1\chi_2^2 - \gamma_2\chi_1^2)]^2 = 0. \quad (18)$$

By studying the variation of this function we note that the system is always stable below threshold (whether $\chi_1^2\gamma_2 > \chi_2^2\gamma_1$ or not) and unstable at threshold (for $\beta^{SS} = \epsilon_c / \gamma_0$). In the special case that $\gamma_1 = \gamma_2 = \gamma_3 = \gamma$ we may find simple analytical solutions as

$$\begin{aligned} \lambda_{1,2} &= \gamma_0, \\ \lambda_{3,4} &= \gamma, \\ \lambda_{5,6} &= \gamma + \frac{\epsilon}{\gamma_0} \sqrt{\chi_1^2 - \chi_2^2}, \\ \lambda_{7,8} &= \gamma - \frac{\epsilon}{\gamma_0} \sqrt{\chi_1^2 - \chi_2^2}. \end{aligned} \quad (19)$$

It is immediately obvious that only $\lambda_{7,8}$ can possibly have a negative real part in this special case, which will happen when

$$\epsilon^2 > \frac{\gamma_0^2 \gamma^2}{\chi_1^2 - \chi_2^2}, \quad (20)$$

and means that any fluctuations will tend to grow, invalidating any linearized fluctuation analysis in this regime. We see that this is consistent with the critical pump value given above, in Eq. (13). We find numerically that the fluctuations above threshold cannot be linearized due to the presence of a zero eigenvalue.

In Fig. 1, we give a plot of the different stability regions, for $\gamma_0 = \gamma_1 = \gamma_3 = 1$, $\gamma_2 = 3\gamma_1$, and $\chi_1 = 0.01\gamma_1$, as χ_2 and ϵ are varied. We see that when the system is oscillating and the nonpump modes are occupied, it is always unstable and must be treated numerically using stochastic equations. In the stable region below and to the right of the solid line we may use a linearized fluctuation analysis to calculate the correlations of interest.

IV. DETECTION OF TRIPARTITE ENTANGLEMENT

There are a number of inequalities whose violation is sufficient to demonstrate the existence of continuous-variable tripartite entanglement, all of which are based on the inseparability of the system density matrix. Unlike bipartite entanglement, where two modes are either entangled or not, there are a number of cases to be considered, depending on possible partitions of the density matrix [31]. In this work we are interested in the case where the density matrix is not separable in any form, often known as genuine tripartite entanglement. Before we describe the criteria we will use here, we need to define the quadrature operators we will use, as different normalizations exist in the literature and can alter the exact form of the inequalities used. As we are considering that the cavity will be at resonance for all modes, we may use the orthogonal quadrature definitions

$$\begin{aligned} \hat{X}_j &= \hat{a}_j + \hat{a}_j^\dagger, \\ \hat{Y}_j &= -i(\hat{a}_j - \hat{a}_j^\dagger), \end{aligned} \quad (21)$$

with the Heisenberg uncertainty principle requiring that $V(\hat{X}_j)V(\hat{Y}_j) \geq 1$. We note here that any cavity detuning or Kerr interaction can change the quadrature angle at which the best quantum correlations are found [32,33], but this is not generally the case for a resonant cavity with $\chi^{(2)}$ interactions.

We will use two different sets of conditions to investigate the presence of entanglement in this system, both of which were described by van Loock and Furusawa [34]. The first of these gives a set of inequalities

$$\begin{aligned} V_{12} &= V(\hat{X}_1 - \hat{X}_2) + V(\hat{Y}_1 + \hat{Y}_2 + g_3\hat{Y}_3) \geq 4, \\ V_{13} &= V(\hat{X}_1 - \hat{X}_3) + V(\hat{Y}_1 + g_2\hat{Y}_2 + \hat{Y}_3) \geq 4, \\ V_{23} &= V(\hat{X}_2 - \hat{X}_3) + V(g_1\hat{Y}_1 + \hat{Y}_2 + \hat{Y}_3) \geq 4, \end{aligned} \quad (22)$$

the violation of any two of which shows that the system is fully inseparable and genuine tripartite entanglement is guaranteed. The g_i are arbitrary real numbers, which may be chosen to minimize the correlations, and will be optimized here as was done in Ref. [15], giving

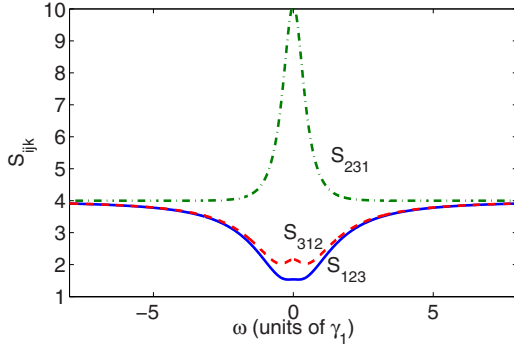


FIG. 2. (Color online) S_{ijk} criteria below threshold for $\epsilon=0.5\epsilon_c$, $\gamma_0=\gamma_1=\gamma_3=1$, and $\gamma_2=3$. In this and all subsequent graphs, the results are dimensionless.

$$\begin{aligned}
 g_1 &= -\frac{V(\hat{Y}_1, \hat{Y}_2) + V(\hat{Y}_1, \hat{Y}_3)}{V(\hat{Y}_1)}, \\
 g_2 &= -\frac{V(\hat{Y}_1, \hat{Y}_2) + V(\hat{Y}_2, \hat{Y}_3)}{V(\hat{Y}_2)}, \\
 g_3 &= -\frac{V(\hat{Y}_1, \hat{Y}_3) + V(\hat{Y}_2, \hat{Y}_3)}{V(\hat{Y}_3)}. \quad (23)
 \end{aligned}$$

The second conditions provide inequalities for which, if any one is violated, genuine tripartite entanglement is demonstrated. They are

$$\begin{aligned}
 V_{123} &= V\left(\hat{X}_1 - \frac{\hat{X}_2 + \hat{X}_3}{\sqrt{2}}\right) + V\left(\hat{Y}_1 + \frac{\hat{Y}_2 + \hat{Y}_3}{\sqrt{2}}\right) \geq 4, \\
 V_{312} &= V\left(\hat{X}_3 - \frac{\hat{X}_1 + \hat{X}_2}{\sqrt{2}}\right) + V\left(\hat{Y}_3 + \frac{\hat{Y}_1 + \hat{Y}_2}{\sqrt{2}}\right) \geq 4, \\
 V_{231} &= V\left(\hat{X}_2 - \frac{\hat{X}_3 + \hat{X}_1}{\sqrt{2}}\right) + V\left(\hat{Y}_2 + \frac{\hat{Y}_3 + \hat{Y}_1}{\sqrt{2}}\right) \geq 4. \quad (24)
 \end{aligned}$$

As in previous cases where the system is described by an asymmetric Hamiltonian (i.e., mode indices cannot be swapped without changing the system), the correct choice of

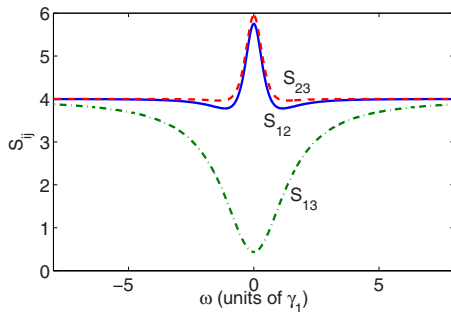


FIG. 3. (Color online) S_{ij} criteria below threshold for $\epsilon=0.5\epsilon_c$, $\gamma_0=\gamma_1=\gamma_3=1$, and $\gamma_2=3$.

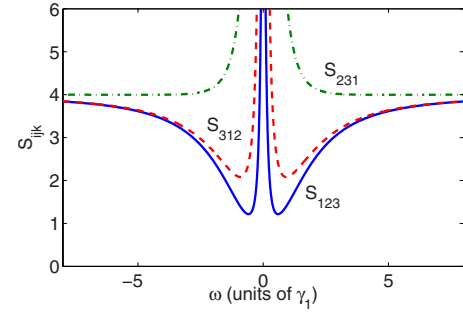


FIG. 4. (Color online) S_{ijk} criteria below threshold with $\epsilon=0.9\epsilon_c$.

indices during the measurement is important for both sets of correlations given above [15].

All these correlations can be simply calculated from the intracavity spectral matrix of Eq. (11) and the use of the standard input-output relations [21] to give the measurable spectra outside the cavity. For example, spectral variances and covariances are calculated as

$$S_{X_j}^{\text{out}}(\omega) = 1 + 2\gamma_j S_{X_j}(\omega),$$

$$S_{X_j X_k}^{\text{out}}(\omega) = 2\sqrt{\gamma_j \gamma_k} S_{X_j X_k}(\omega), \quad (25)$$

and similarly for the \hat{Y} quadratures. As this notation can become rather clumsy, we will use S_{ij} and S_{ijk} in what follows to refer to the output spectral qualities equivalent to the V_{ij} and V_{ijk} correlations defined above. The same inequalities hold for these.

V. SPECTRAL RESULTS IN THE STABLE REGIME

Although it is possible to obtain analytical results for the S_{ij} and S_{ijk} , these are extremely unwieldy and not at all enlightening. We have therefore chosen to present the results graphically for various parameter regimes. We note here that we have not chosen our parameters to represent any particular experimental values, as technological progress in the engineering of nonlinear crystals can now make a wide range of nonlinearities available to the experimentalist. Rather than do this, we have chosen to use a representative range of

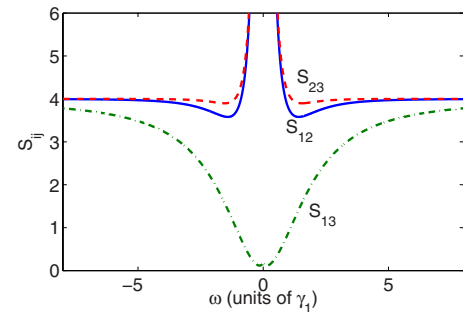


FIG. 5. (Color online) S_{ij} criteria below threshold with $\epsilon=0.9\epsilon_c$.

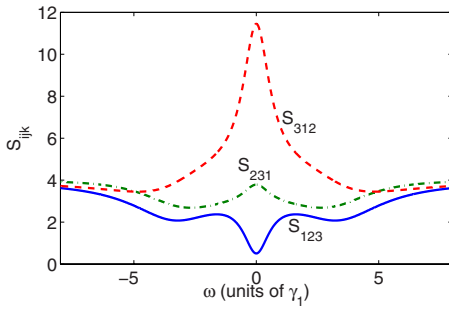


FIG. 6. (Color online) S_{ijk} criteria for the system without threshold, with $\epsilon=1.5\epsilon_c^o$.

parameters in the three different regimes and note that once the loss rate is known for a particular cavity at ω_1 , everything may be scaled by this, as we will always set $\gamma_1=1$ in what follows.

In Figs. 2 and 3, we show the results for the two different types of correlations at half the critical pumping amplitude, in the regime where $\chi_2=0.4\chi_1$ and with the loss rates set as $\gamma_0=\gamma_1=\gamma_3=1$, and $\gamma_2=3$. In all results presented here we have used a value of $\chi_1=0.01$. In Fig. 2 we see clear evidence of genuine tripartite entanglement, with both S_{123} and S_{312} obviously violating the inequality, with only one of these being below 4 already being sufficient. In Fig. 3, where two of the inequalities need to be violated, we see that S_{12} and S_{13} both show entanglement, although not over as large a frequency region as the S_{ijk} . As in Ref. [15], this is a result of the asymmetry of the Hamiltonian and the fact that a violation of the tripartite inequalities is a sufficient but not necessary condition for the demonstration of tripartite entanglement.

We see in Figs. 4 and 5 that, with $\epsilon=0.9\epsilon_c$, the violation of the inequalities has increased for two of the S_{ijk} , with the spectra bifurcating so that no entanglement is seen at near zero frequency. The S_{ij} also show increased violation as the threshold is approached, but again not near zero frequency. The S_{ij} again do not indicate full inseparability over as wide a frequency range as the S_{ijk} .

In the region without an oscillation threshold, that is $\chi_2 \geq \sqrt{\gamma_2/\gamma_1}\chi_1$, we may also apply the linearized analysis. In Figs. 6 and 7 we show the correlation functions for $\chi_2=2.5\chi_1$, with $\epsilon=1.5\epsilon_c^o$ and the other parameters unchanged

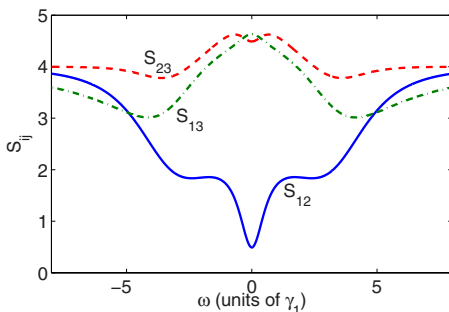


FIG. 7. (Color online) S_{ij} criteria for the system without threshold, with $\epsilon=1.5\epsilon_c^o$.

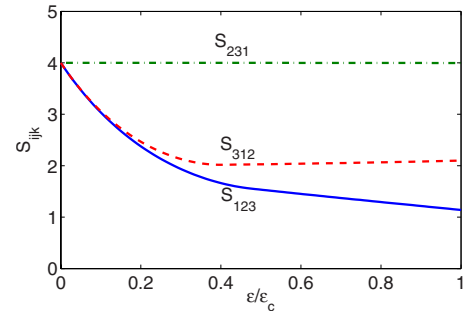


FIG. 8. (Color online) Minimum of the S_{ijk} at any frequency between 0 and $10\gamma_0$ as the pump varies up to ϵ_c in the region with threshold.

from Fig. 2. We see that entanglement is found in this regime and that its demonstration is less dependent on which particular correlations are measured, although S_{312} and S_{23} do not violate the inequality by a large amount. The main conclusion to be drawn from these results is that the S_{ijk} correlations are the most appropriate to use for this system, with S_{123} giving the maximum violation of the inequalities.

We will now investigate the effects of changing ϵ on the correlations, concentrating on the S_{ijk} , as these have proven to be a more sensitive measure than the S_{ij} . We first examine the region that has a threshold, that is where $\epsilon < \epsilon_c$ and $\chi_2 < \chi_1\sqrt{\gamma_2/\gamma_1}$. We will present these results at the frequency of maximum violation of the inequalities, with the range $0 \leq \omega \leq \gamma_0$, rather than fixing the frequency as the other parameters are changed. In Fig. 8 we show the minima of the three S_{ijk} as the pump varies between zero and the critical value, with $\chi_1=0.01$, $\chi_2=0.4\chi_1$, $\gamma_0=\gamma_1=\gamma_3=1$, and $\gamma_2=3$. We see that in no case does S_{231} violate the inequality, while the other two show clear violations, with S_{123} decreasing as threshold is approached. We note here that the results in the immediate neighborhood of the threshold are not expected to be accurate, due to the invalidity of the linearized fluctuation analysis at that point.

In the parameter regime where there is no oscillation threshold, we can also investigate the effects of varying both the pumping and χ_2 . We again set $\gamma_0=\gamma_1=\gamma_3=1$, $\gamma_2=3$, and $\chi_1=0.01$, and will allow ω to vary so as to find the maximal violations. In Figs. 9 and 10, we plot the S_{ijk} as a function of ϵ/ϵ_c^o , for values of $\chi_2=2\chi_1$ and $3\chi_1$. We again see that S_{123}

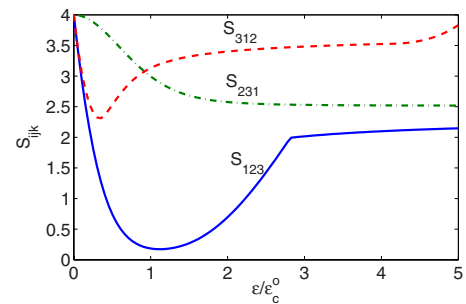


FIG. 9. (Color online) Tripartite entanglement criteria for the system without threshold, with $\gamma_0=\gamma_1=\gamma_3=1$, $\gamma_2=3$, $\chi_1=0.01$, and $\chi_2=2\chi_1$.

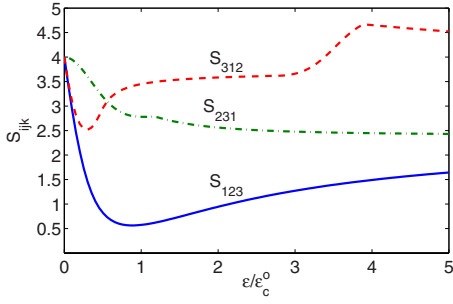


FIG. 10. (Color online) Tripartite entanglement criteria for the system without threshold, with $\gamma_0 = \gamma_1 = \gamma_3 = 1$, $\gamma_2 = 3$, $\chi_1 = 0.01$, and $\chi_2 = 3\chi_1$.

gives the maximal violations, although this does not increase monotonically with pump amplitude. In Figs. 11 and 12 we show how the correlations, again at the optimal frequencies, change as χ_2 is increased from $\chi_2^{\text{crit}} (= \chi_1 \sqrt{\gamma_2 / \gamma_1})$, for two different pumping amplitudes. We again see clear evidence of genuine tripartite entanglement over the range shown, with S_{123} again showing the maximum violations of the inequality. We note that the violations do not increase as χ_2 increases, but that S_{123} has its minima at χ_2^{crit} .

The results found from our semiclassical analysis show a range of different behaviors, including threshold behavior which depends on an interplay of the two nonlinearities and could not be found in the undepleted pump treatment of Ref. [19]. We have been able to demonstrate that genuine tripartite entanglement is available for a wide range of parameters but have not been able to analyze the system in the above

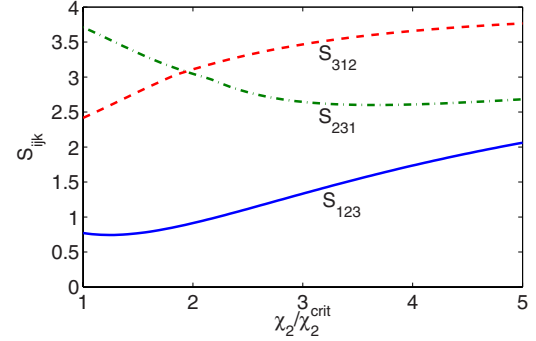


FIG. 11. (Color online) Tripartite entanglement criteria for the system without threshold, with $\gamma_0 = \gamma_1 = \gamma_3 = 1$, $\gamma_2 = 3$, $\chi_1 = 0.01$, and $\epsilon = 0.5\epsilon_c^0$. The results are plotted as a function of $\chi_2^{\text{crit}} = \chi_1 \sqrt{\gamma_2 / \gamma_1}$.

threshold regime, due to phase diffusion of the modes and the inapplicability of the linearization procedure. In order to investigate the behavior above threshold we will now turn to numerical stochastic integration.

VI. STOCHASTIC INTEGRATION IN THE UNSTABLE REGIME

In this case the numerical integration of the full positive- P equations [Eq. (6)] presents stability problems, so that, although they were useful in deriving the correct linearized equations to calculate normally ordered correlation functions, we will now turn to what is known as the truncated Wigner representation [29]. Following the standard procedures [24], the generalized Fokker-Planck equation for the Wigner representation pseudoprobability function of the system is found as

$$\begin{aligned} \frac{dW}{dt} = & \left\{ - \left[\frac{\partial}{\partial \alpha_1} (\gamma_1 \alpha_1 - \chi_1 \alpha_3^* \beta) + \frac{\partial}{\partial \alpha_1^*} (\gamma_1 \alpha_1^* - \chi_1 \alpha_3 \beta^*) + \frac{\partial}{\partial \alpha_2} (\gamma_2 \alpha_2 - \chi_2 \alpha_3 \beta) \right. \right. \\ & + \frac{\partial}{\partial \alpha_2^*} (\gamma_2 \alpha_2^* - \chi_2 \alpha_3^* \beta^*) + \frac{\partial}{\partial \alpha_3} (\gamma_3 \alpha_3 - \chi_1 \alpha_1^* \beta + \chi_2 \alpha_2 \beta^*) + \frac{\partial}{\partial \alpha_3^*} (\gamma_3 \alpha_3^* - \chi_1 \alpha_1 \beta^* + \chi_2 \alpha_2^* \beta) \\ & \left. \left. + \frac{\partial}{\partial \beta} (\gamma_0 \beta - \epsilon + \chi_1 \alpha_1 \alpha_3 + \chi_2 \alpha_2 \alpha_3^*) + \frac{\partial}{\partial \beta^*} (\gamma_0 \beta^* - \epsilon^* + \chi_1 \alpha_1^* \alpha_3^* + \chi_2 \alpha_2^* \alpha_3) \right] \right. \\ & + \frac{1}{2} \left[\frac{\partial^2}{\partial \alpha_1 \partial \alpha_1^*} (2\gamma_1) + \frac{\partial^2}{\partial \alpha_2 \partial \alpha_2^*} (2\gamma_2) + \frac{\partial^2}{\partial \alpha_3 \partial \alpha_3^*} (2\gamma_3) + \frac{\partial^2}{\partial \beta \partial \beta^*} (2\gamma_0) \right] \\ & \left. - \frac{1}{8} \left[\frac{\partial^3}{\partial \alpha_2 \partial \alpha_3^* \partial \beta^*} (2\chi_2) + \frac{\partial^3}{\partial \alpha_2^* \partial \alpha_3 \partial \beta} (2\chi_2) - \frac{\partial^3}{\partial \alpha_1 \partial \alpha_3 \partial \beta^*} (2\chi_1) - \frac{\partial^3}{\partial \alpha_1^* \partial \alpha_3^* \partial \beta} (2\chi_1) \right] \right\} W. \end{aligned} \quad (26)$$

We immediately see that the above equation contains third-order derivatives so that it cannot be mapped onto a set of stochastic differential equations. Although methods have been developed to map this type of generalized Fokker-Planck equations onto stochastic difference equations in a doubled phase space [35], the integration of these can present

more stability problems than the positive- P representation, so we will not pursue this approach here. A commonly used approximation that has been shown to give good results for a number of nonlinear systems [36,37] is to truncate the generalized Fokker-Planck equation at second order. This may be heuristically justified in this case by the fact that the sec-

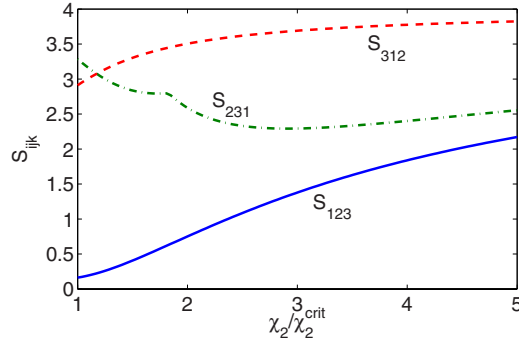


FIG. 12. (Color online) Tripartite entanglement criteria for the system without threshold, with $\gamma_0 = \gamma_1 = \gamma_3 = 1$, $\gamma_2 = 3$, $\chi_1 = 0.01$, and $\epsilon = 0.9\epsilon_c$. The results are plotted as a function of $\chi_2^{\text{crit}} = \chi_1 \sqrt{\gamma_2} / \gamma_1$.

ond order terms, which will be proportional to the square roots of the loss rates in the stochastic equations, are much larger than the third order terms, which will be proportional to the cube roots of the nonlinearities. Hence we neglect the third-order derivatives to allow a mapping onto the set of stochastic equations in the truncated Wigner representation

$$\begin{aligned} \frac{d\alpha_1}{dt} &= -\gamma_1 \alpha_1 + \chi_1 \alpha_3^* \beta + \sqrt{\frac{\gamma_1}{2}} (\eta_1 + i\eta_2), \\ \frac{d\alpha_2}{dt} &= -\gamma_2 \alpha_2 + \chi_2 \alpha_3 \beta + \sqrt{\frac{\gamma_2}{2}} (\eta_3 + i\eta_4), \\ \frac{d\alpha_3}{dt} &= -\gamma_3 \alpha_3 + \chi_1 \alpha_1^* \beta - \chi_2 \alpha_2 \beta^* + \sqrt{\frac{\gamma_3}{2}} (\eta_5 + i\eta_6), \\ \frac{d\beta}{dt} &= \epsilon - \gamma_0 \beta - \chi_1 \alpha_1 \alpha_3 - \chi_2 \alpha_2 \alpha_3^* + \sqrt{\frac{\gamma_0}{2}} (\eta_7 + i\eta_8), \end{aligned} \quad (27)$$

where the η_j are Gaussian random noises as defined by Eq. (7). As well as not containing multiplicative noise terms, another important difference from the positive- P equations is that the initial conditions on each stochastic trajectory must be drawn from the appropriate Wigner distribution for the desired quantum state of the mode. We will be beginning our trajectories with vacuum inside the cavity, so that, for example, we choose $\alpha_i^n(0) = (\xi_1^n + i\xi_2^n)/2$ on the n th trajectory [and similarly for $\beta(0)$], where the ξ are normal Gaussian random numbers with zero mean. The Wigner representation naturally calculates symmetrically ordered operator averages, so that care must be taken with any necessary reordering to give predictions for observables. We also note here that, while cases have been found where the truncated Wigner representation can give inaccurate results [38,39], we expect it to be accurate here because all four modes are macroscopically occupied in the region that we are using it to investigate. It is also worth noting that the quantities which were calculated in Refs. [38,39] were not the single-time correlation functions that we calculate here and that we do not know of any example where the truncated Wigner has given erroneous results for this type of correlation. In our stochastic

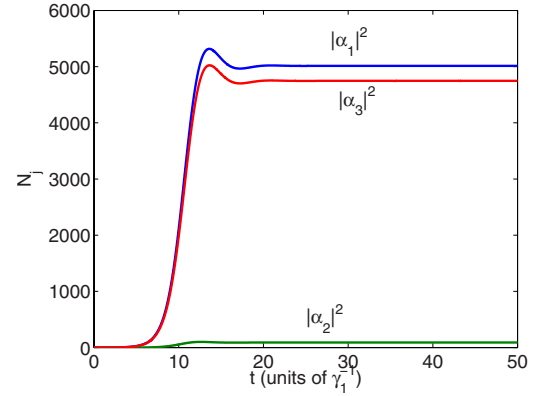


FIG. 13. (Color online) Intensity of the output modes $|\alpha_i|^2$, obtained by stochastic integration of the truncated Wigner equations averaged over 2.65×10^5 trajectories. Note that the horizontal axis is now time scaled in units of γ_1^{-1} .

integration we have set $\gamma_0 = \gamma_1 = \gamma_3 = 1$, $\gamma_2 = 3\gamma_1$, $\chi_1 = 0.01\gamma_1$, $\chi_2 = 0.4\chi_1$, and $\epsilon = 1.5\epsilon_c$. An indication of the accuracy is that it gives predictions for the intracavity field intensities that are consistent with the analytical values given above, as shown in the table, thereby lending more justification to the use of this approximate method.

	Analytic	Wigner
$ \beta ^2$	1.056×10^4	1.056×10^4
$ \alpha_1 ^2$	5.0143×10^3	5.0141×10^3
$ \alpha_2 ^2$	89.1424	89.0909
$ \alpha_3 ^2$	4.7468×10^3	4.7471×10^3

In Figs. 13 and 14 we show the intensity of the α modes inside the cavity, demonstrating both that we have reached the steady-state regime and that the modes are macroscopically occupied. Integration for values of ϵ close to ϵ_c typically took much longer to reach the steady state, due to critical slowing down, a well-known phenomenon that occurs in the vicinity of phase transitions. Due to the phase diffusion

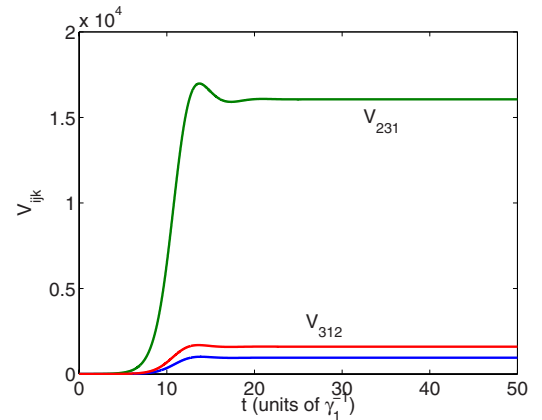


FIG. 14. (Color online) The V_{ijk} for $\epsilon = 1.5\epsilon_c$, obtained by stochastic integration of the truncated Wigner equations averaged over 2.65×10^5 trajectories. Note that the horizontal axis is now time scaled in units of γ_1^{-1} .

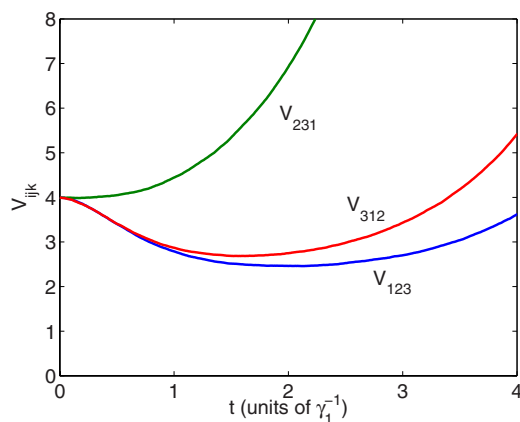


FIG. 15. (Color online) Transient behavior of the V_{ijk} with $\epsilon = 1.5\epsilon_c$. As seen in Fig. 13, the violations of the inequalities persist for only a short time.

predicted in the analytical solutions, the averages of the α_j are essentially zero and no entanglement is registered by the V_{ijk} correlations in the steady state, with these all being far from violating the inequalities. As shown in Fig. 15, there is some violation in the initial transient regime before the pump mode within the cavity builds up to its threshold value and the system begins to oscillate. This transient feature is unlikely to be of any practical use, as it exists for only a few cavity lifetimes and the fields are no more intense than in the below threshold regime, where genuine tripartite entanglement is readily seen in the steady-state regime. We note here that the three-mode EPR correlations [18] give much smaller values in the steady state, but still do not violate the inequalities. It is possible that a small injected signal at ω_2 could serve to lock the phases and enable entanglement to be ob-

served, but investigation of this is outside the scope of the present work.

VII. CONCLUSION

We have analyzed the system of singly pumped intracavity coupled down-conversion and sum-frequency generation with a quantized pump field. Unlike previous analyses, this enabled us to define the threshold properties of the system and analyze the dynamics with all modes oscillating macroscopically inside the cavity. One of the features we have found is that for some values of the experimental parameters, the threshold value of the pump field diverges so that, however strongly the cavity is pumped, the system will not oscillate. We have found that genuine tripartite entanglement is available in both the regions below and without threshold, but that, as in other systems with asymmetric Hamiltonians, not all measurable correlations will detect the violation of the entanglement inequalities. Above threshold the converted modes undergo phase diffusion, which prevents the detection of entanglement based on quadrature measurements except in the early transient regime. This signifies that the system is not a good candidate for the production of bright entangled output beams, unless a method can be found to overcome the problem of phase diffusion. However, it is still useful for the production of genuine polychromatic tripartite entanglement in all except the above threshold regime.

ACKNOWLEDGMENTS

This work was supported by the Australian Research Council and the Queensland state government. C. Pennarun was a guest of the University of Queensland with financial support from the French government programme Explo'ra Sup.

-
- [1] A. Einstein, B. Podolsky, and N. Rosen, *Phys. Rev.* **47**, 777 (1937).
 - [2] M. D. Reid, *Phys. Rev. A* **40**, 913 (1989).
 - [3] Z. Y. Ou, S. F. Pereira, H. J. Kimble, and K. C. Peng, *Phys. Rev. Lett.* **68**, 3663 (1992).
 - [4] C. H. Bennett, G. Brassard, C. Crépeau, R. Jozsa, A. Peres, and W. K. Wootters, *Phys. Rev. Lett.* **70**, 1895 (1993).
 - [5] D. Bouwmeester, J.-W. Pan, K. Mattle, M. Eibl, H. Weinfurter, and A. Zeilinger, *Nature (London)* **390**, 575 (1997).
 - [6] S. L. Braunstein and H. J. Kimble, *Phys. Rev. Lett.* **80**, 869 (1998).
 - [7] S. L. Braunstein and P. van Loock, *Rev. Mod. Phys.* **77**, 513 (2005).
 - [8] J. Jing, J. Zhang, Y. Yan, F. Zhao, C. Xie, and K. Peng, *Phys. Rev. Lett.* **90**, 167903 (2003).
 - [9] T. Aoki, N. Takei, H. Yonezawa, K. Wakui, T. Hiraoka, A. Furusawa, and P. van Loock, *Phys. Rev. Lett.* **91**, 080404 (2003).
 - [10] A. S. Villar, M. Martinelli, C. Fabre, and P. Nussenzveig, *Phys. Rev. Lett.* **97**, 140504 (2006).
 - [11] A. Ferraro, M. G. A. Paris, M. Bondani, A. Allevi, E. Puddu, and A. Andreoni, *J. Opt. Soc. Am. B* **21**, 1241 (2004).
 - [12] J. Guo, H. Zou, Z. Zhai, J. Zhang, and J. Gao, *Phys. Rev. A* **71**, 034305 (2005).
 - [13] M. K. Olsen and A. S. Bradley, *J. Phys. B* **39**, 127 (2006).
 - [14] M. Bondani, A. Allevi, E. Gevinti, A. Agliati, and A. Andreoni, *Opt. Express* **14**, 9838 (2006).
 - [15] M. K. Olsen and A. S. Bradley, *Phys. Rev. A* **74**, 063809 (2006).
 - [16] O. Pfister, S. Feng, G. Jennings, R. C. Pooser, and D. Xie, *Phys. Rev. A* **70**, 020302(R) (2004).
 - [17] A. S. Bradley, M. K. Olsen, O. Pfister, and R. C. Pooser, *Phys. Rev. A* **72**, 053805 (2005).
 - [18] M. K. Olsen, A. S. Bradley, and M. D. Reid, *J. Phys. B* **39**, 2515 (2006).
 - [19] Y. B. Yu, Z. D. Xie, X. Q. Yu, H. X. Li, P. Xu, H. M. Yao, and S. N. Zhu, *Phys. Rev. A* **74**, 042332 (2006).
 - [20] M. E. Smithers and E. Y. C. Lu, *Phys. Rev. A* **10**, 1874 (1974).
 - [21] C. W. Gardiner and M. J. Collett, *Phys. Rev. A* **31**, 3761 (1985).
 - [22] M. K. Olsen, *Phys. Rev. A* **70**, 035801 (2004).
 - [23] P. D. Drummond and C. W. Gardiner, *J. Phys. A* **13**, 2353

- (2003).
- [24] C. W. Gardiner, *Quantum Noise* (Springer, Berlin, 1991).
- [25] D. F. Walls and G. J. Milburn, *Quantum Optics* (Springer, Berlin, 1994).
- [26] R. J. Glauber, Phys. Rev. **131**, 2766 (1963).
- [27] E. C. G. Sudarshan, Phys. Rev. Lett. **10**, 277 (1963).
- [28] C. W. Gardiner, *Handbook of Stochastic Methods* (Springer, Berlin, 1985).
- [29] R. Graham, in *Quantum Statistics in Optics and Solid-State Physics*, edited by G. Hohler, Vol. 66 of *Springer Tracts in Modern Physics* (Springer, New York, 1973).
- [30] M. D. Reid and P. D. Drummond, Phys. Rev. A **40**, 4493 (1989).
- [31] G. Giedke, B. Kraus, M. Lewenstein, and J. I. Cirac, Phys. Rev. A **64**, 052303 (2001).
- [32] M. K. Olsen, S. C. G. Granja, and R. J. Horowicz, Opt. Commun. **165**, 293 (1999).
- [33] M. K. Olsen, Phys. Rev. A **73**, 053806 (2006).
- [34] P. van Loock and A. Furusawa, Phys. Rev. A **67**, 052315 (2003).
- [35] L. I. Plimak, M. K. Olsen, M. Fleischhauer, and M. J. Collett, Europhys. Lett. **56**, 372 (2001).
- [36] M. J. Steel, M. K. Olsen, L. I. Plimak, P. D. Drummond, S. M. Tan, M. J. Collett, D. F. Walls, and R. Graham, Phys. Rev. A **58**, 4824 (1998).
- [37] A. A. Norrie, R. J. Ballagh, C. W. Gardiner, and A. S. Bradley, Phys. Rev. A **73**, 043618 (2006).
- [38] P. D. Drummond and P. Kinsler, Phys. Rev. A **40**, 4813 (1989).
- [39] M. K. Olsen, K. Dechoum, and L. I. Plimak Opt. Commun. **190**, 261 (2001).